

TAMING CONTINUOUS SPURIOUS SHIFT IN DOMAIN ADAPTATION

Anonymous authors

Paper under double-blind review

ABSTRACT

Recent advances in domain adaptation have shown promise in transferring knowledge across domains characterized by a continuous value or vector, such as varying patient ages, where “age” serves as a continuous index. However, these approaches often fail when spurious features shift continuously along with the domain index. This paper introduces the first method designed to withstand the continuous shifting of spurious features during domain adaptation. Our method enhances domain adaptation performance by aligning causally transportable encodings across continuously indexed domains. Theoretical analysis demonstrates that our approach more effectively ensures causal transportability across different domains. Empirical results, from both semi-synthetic and real-world medical datasets, indicate that our method outperforms state-of-the-art domain adaptation methods.

1 INTRODUCTION

Machine learning typically presumes that the training and test data comes from identical distributions, hoping that the trained model effectively generalizes to the test environment. However, this presumption breaks when the training and testing occur across different domains (e.g., with distinct source and target domains). Domain adaptation (DA) effectively addresses this challenge by utilizing labeled data from the source domain along with either unlabeled or minimally labeled data from the target domain, thereby improving model performance (Ben-David et al., 2010; Ganin et al., 2016; Tzeng et al., 2017; Zhang et al., 2019).

Continuously indexed domain adaptation (CIDA) (Wang et al., 2020) generalizes typical DA, which focuses on discrete domains (transferring from dataset A to B), to DA across continuously indexed domains, where domain shift is characterized by a continuous index such as time and location. For instance, in healthcare, CIDA can be instrumental in transferring knowledge across patient data that varies with age. As patients age, their physiological parameters and response to treatments can change subtly; in response, CIDA aims to train a model that can adapt to these continuous shifts. Unfortunately, previous DA methods (Ganin et al., 2016; Tzeng et al., 2017; Zhang et al., 2019), including CIDA (Wang et al., 2020), often fail when spurious features are continuously shifting.

Example 1 (Continuously Shifting Spurious Features in Sleep Studies). *Suppose one trains a model to take as input a time series of breathing signal $\mathbf{x} \in \mathbb{R}^T$ to predict the corresponding sleep stage as $y^{pred} \in \{\text{‘Awake’}, \text{‘Light Sleep’}, \text{‘Deep Sleep’}, \text{‘REM Sleep’}\}$. Here ‘respiratory rate’ is a typical spurious feature. If one trains the model using data from young subjects (with age 20 ~ 30), it will learn that ‘higher respiratory rates’ often correspond to ‘REM Sleep’. However, as subjects continuously age, they may have a slower respiratory rate in breathing patterns. Therefore the spurious feature ‘respiratory rate’ no longer works when predicting sleep stages for older subjects, and the older the subject is, the lower the model accuracy.*

Our analysis shows that either alignment-based methods (Ganin et al., 2016; Wang et al., 2020) or causality-inspired methods (Mao et al., 2022) alone do not solve the problem. Alignment-based methods tend to align spurious features rather than causal features, therefore often fail to generalize across continuously indexed domains with continuously shifting spurious features. On the other hand, causality-inspired methods aiming to learn causal features (encodings) may collapse to non-causal (association-based) methods (see Sec. 3 for detailed analysis), therefore also failing to generalize. Motivated by such analysis, we then propose to jointly (1) infer causally transportable

Table 1: Comparison of our CADA with different representative previous methods.

	CUA	ADDA	DANN	CDANN	MDD	CIDA	VOOD	CADA (Ours)
Continuous	✗	✗	✗	✗	✗	✓	✗	✓
Causal	✗	✗	✗	✗	✗	✗	✓	✓
Multi-Domain	✓	✗	✓	✓	✗	✓	✗	✓
Covariate Shift	✓	✓	✓	✓	✓	✓	✗	✓
Setting (DA/DG)	DA	DA	DA	DA	DA	DA	DG	DA

encodings (representations) and (2) align these encodings across continuously indexed domains, thereby improving domain adaptation performance under continuous spurious shift. Our contributions are as follows:

- We identify the problem of continuous spurious shift and propose Continuously trAnsportable Domain Adaptation (CADA) as the first general DA method to address this problem.
- Our theoretical analysis shows that our CADA can better ensure causal transportability across continuously indexed domains.
- Empirical results on both semi-synthetic and real-world medical datasets show that our method outperforms the state-of-the-art DA methods in the face of continuous spurious shift.

2 RELATED WORK

Typical Domain Adaptation. Domain Adaptation has long been studied (Farahani et al., 2021; Csurka, 2017; Ben-David et al., 2010; Peng et al., 2019; Prabhu et al., 2021; Liu et al., 2023; Xu et al., 2022) to promote model’s generalization ability on unseen domains, with unlabeled or a limited amount of labeled data. Traditional methods include importance weighting (Shimodaira, 2000; Gretton et al., 2009; Lipton et al., 2018), self-training (Zou et al., 2018; Kumar et al., 2020; Prabhu et al., 2021), distribution matching (Pan et al., 2010; Tzeng et al., 2014; Sun & Saenko, 2016; Peng et al., 2019; Nguyen-Meidine et al., 2021) and adversarial-based training (Ganin et al., 2016; Zhang et al., 2019; Zhao et al., 2017; Wang et al., 2020; Xu et al., 2023). Typically, these methods focus on categorical domains, where an one-hot vector indicates which domain a data point comes from. In contrast, CIDA (Wang et al., 2020) extends to continuous domains, with a continuous variable specifying each data point’s domain. CIDA seeks to align encodings of different domain based on this continuous identification. However, during the alignment, CIDA struggles to eliminate the influence of continuously shifting spurious features, leading to poor performance (see empirical results in Sec. 5). In contrast, our method successfully mitigates the impact of such spurious features by inferring and aligning causally transportable representations.

Causality-Inspired Domain Adaptation. Causal inference is a powerful method for modeling knowledge transfer (Bareinboim & Pearl, 2014; 2013; 2016; Bühlmann, 2020; Correa & Bareinboim, 2019; 2020; Magliacane et al., 2018; Rojas-Carulla et al., 2018) and ensuring structure invariance (Pearl et al., 2000). Various studies have explored its application to eliminate spurious features and improve domain adaptation performance (Arjovsky et al., 2019; Mahajan et al., 2021; Mao et al., 2021; Yue et al., 2021). For instance, VOOD (Mao et al., 2022) aims to estimate invariant causal effect across different environments, hoping to improve domain generalization (DG) performance. However, these causal methods (1) are still subject to covariate shift, often compromising the causal model’s identifiability (Pearl et al., 2000), (2) can easily degenerate to association-based method, and (3) are not designed for continuously indexed domains. In contrast, our CADA effectively addresses these problem via joint latent-space distribution alignment and causal inference.

Comparison of Representative Methods. Table 1 summarizes the differences between our CADA and representative previous methods in terms of whether they (1) are designed for continuously indexed domains, (2) are causal/robust against spurious features, (3) can naturally handle multiple source/target domains, (4) are robust against covariate shift, and (5) are designed for DA or DG.

3 THEORETICAL ANALYSIS

In this section, we describe the challenges of performing domain adaptation on data with continuously shifting spurious correlations. We then present the solution in Sec. 4. **All proofs are available in Appendix A.**

Notation and Problem. We consider the problem of unsupervised continuously indexed domain adaptation as proposed in (Wang et al., 2020). We assume that the continuous domain index set \mathcal{K} is a part of a metric space, $\mathcal{K} = \mathcal{K}_s \cup \mathcal{K}_t$, with \mathcal{K}_s and \mathcal{K}_t as domain index sets for the source and target domains, respectively. The input and labels are denoted as \mathbf{x} and y , respectively. Given the labeled source-domain data $(\mathbf{x}_i^s, y_i^s, k_i^s)_{i=1}^n$ and unlabeled target-domain data $(\mathbf{x}_i^t, k_i^t)_{i=1}^l$, with $k_i^s \in \mathcal{K}_s$ and $k_i^t \in \mathcal{K}_t$, the goal is to predict the target-domain labels $(y_i^t)_{i=1}^l$. (Note that the labels $(y_i^t)_{i=1}^l$ are only available at test time for evaluation purpose only.) We use upper-case letters (e.g., X) to denote random variables and lower-case letters (e.g., x) to denote corresponding realizations.

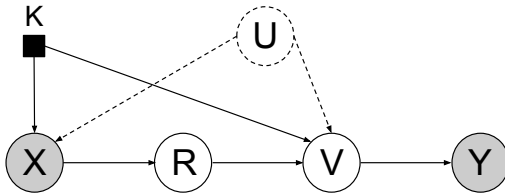


Figure 1: Causal diagram for CADA. Shaded nodes denote observed variables.

3.1 A CAUSAL VIEW ON CONTINUOUSLY INDEXED DOMAIN ADAPTATION

Structural Causal Model. We use the Structural Causal Model (SCM) in Fig. 1 to describe the underlying generative process of the random variables the data X and their labels Y . In addition to the observed variables X and Y , this SCM also involves the following variables:

- R , which is a vector encoding both causal and spurious features of the input data X ,
- V , which is the input’s causal factors extracted from the representation R ,
- U , which is the unobserved noise and spurious features from external sources, and
- K , which is the continuous domain index.

U and K together affect both the generation of input X and the extraction of causal factors V from R ; in other words, U and K guide the process of eliminating spurious features from R . Note that in the context of causal inference, K can be considered as a continuous version of the *transportability node* (Pearl & Bareinboim, 2011); it points to variables whose generation process differs for different domains.

Following Example 1, below we provide an example of using the SCM in Fig. 1 for sleep studies across continuously indexed domains (patients of different ages).

Example 2 (Causal Model for Sleep Studies). In sleep studies (Zhao et al., 2017), one typical task is to estimate the sleep stage Y (e.g., “Awake” and “Deep Sleep”) from a patient’s breathing signal X ; here “age” is a domain index K ; patients of different ages belong to different domains. One robust way to predict Y is to use breathing patterns such as periodicity (periodic breathing signals usually indicate “Deep Sleep”); these patterns are encoded as **causal representations** V in our CADA. The unobserved **spurious features** U in sleep studies may include ‘respiratory rate’ mentioned in Example 1. Breathing signals X from older patients, i.e., larger K , may have a lower ‘respiratory rate’ due to weakened respiratory muscles; therefore it is **not a reliable feature** for predicting Y . A neural network can extract the compact representation R given the raw breathing signal X as input, but R still inherits the spurious features U from X ; therefore directly using R to predict Y would not generalize across domains (different K), as in Example 1. To address this problem, we would like to remove the spurious features U from R according to K , thereby obtaining the causal factors/representations V . We can then train a generalizable (and causally transportable) model to predict sleep stages Y using the causal representations V .

3.2 CHALLENGES IN CONTINUOUSLY TRANSPORTABLE DOMAIN ADAPTATION

Conditional Model $P(Y|X)$ Is Not Generalizable across Domains. Due to the confounding factors K and U between X and V , the computable quantity $P(Y|X)$ trained in source domains usually do not generalize to target domains, i.e. $P(Y|X, K = k_1) \neq P(Y|X, K = k_2)$ for $k_1 \neq k_2 \in \mathcal{K}$.

Causal Model $P(Y|do(X))$ Is Generalizable across Domains. Fortunately, with the causal graph in Fig. 1, the causal effect $P(Y|do(X))$ is transportable (and generalizable) across different domains. This is demonstrated in Theorem 3.1 and Theorem 3.2 below.

Theorem 3.1 (Transportability of $P(v|do(x))$). *With the causal diagram in Fig. 1, the causal relation $P(v|do(x))$ is transportable from domain k_1 to k_2 for any $k_1 \neq k_2$.*

Theorem 3.2 (Transportability of $P(y|do(x))$). *With the causal diagram in Fig. 1, the causal relation $P(y|do(x))$ is trivially transportable from domain k_1 to k_2 for any $k_1 \neq k_2$ using:*

$$P(y|do(x)) = \sum_v P(y|v)Q(v|x), \quad (1)$$

where $Q(v|x)$ is an probabilistic encoder generating encoding v given the input x . It is constructed as

$$Q(v|x) = \sum_r P(r|x) \sum_{x'} P(v|r, x')P(x'). \quad (2)$$

Transportability Alone Is Not Sufficient. From Eqn. 1, we can see that v computed from Eqn. 2 can be treated as the encoding for the input x . In practice, due to covariate shift (Ganin et al., 2016; Ben-David et al., 2010), there is no guarantee that directly using Eqn. 1 will lead to good domain adaptation performance. Specifically, Eqn. 2 may theoretically guarantee causal correlation learning, such guarantees break in the presence of covariate shift, which leads to non-positivity in variable V 's probability distributions and non-identifiability of the causal interventional distribution $P(V|do(X))$ (Definition 3.2.3 and Definition 3.2.4 of (Pearl et al., 2000)). The following lemma adapted from (Ben-David et al., 2010) shows the consequence of covariate shift.

Lemma 3.1 (Target-Domain Error Bound). *Let \mathcal{H} be a hypothesis space, and $h \in \mathcal{H} : \mathcal{V} \rightarrow \{0, 1\}$. $\mathcal{D}_S(V)$ and $\mathcal{D}_T(V)$ are the encoding distributions of the source and target domains, respectively. We have:*

$$\epsilon_{\mathcal{D}_T}(h) \leq \epsilon_{\mathcal{D}_S}(h) + \frac{1}{2}d_{\mathcal{H}\Delta\mathcal{H}}(\mathcal{D}_S(V), \mathcal{D}_T(V)) + \lambda,$$

where $\epsilon_{\mathcal{D}_S}(h)$ and $\epsilon_{\mathcal{D}_T}(h)$ are the prediction error in the source and target domains, respectively. The constant $\lambda = \min_h(\epsilon_{\mathcal{D}_S}(h) + \epsilon_{\mathcal{D}_T}(h))$. The $\mathcal{H}\Delta\mathcal{H}$ divergence $d_{\mathcal{H}\Delta\mathcal{H}}(\mathcal{D}_S(V), \mathcal{D}_T(V))$ characterizes the divergence between the source domain's and the target domain's encoding distributions.

Lemma 3.1 shows that the generalization error of a target domain is bounded by the source-domain error, the distribution divergence between the encoding v of the source and target domains, and the constant λ . Therefore it is also important to reduce the second term $d_{\mathcal{H}\Delta\mathcal{H}}(\mathcal{D}_S(V), \mathcal{D}_T(V))$ by aligning the encoding distributions of v from different domains.

Definition 1 (Ideal Encoder $Q(v|x)$). *With the analysis above, an ideal encoder $Q(v|x)$ that encodes the input x into an encoding v is an encoder that*

- (1) has the form of Eqn. 2 and
- (2) ensures the marginal independence $k \perp\!\!\!\perp v$.

The first requirement in Definition 1 is trivially satisfied by construction. However, with v generated by $Q(v|x)$ in Eqn. 2, there is no guarantee that $k \perp\!\!\!\perp v$ (the second requirement in Definition 1); this is shown in Theorem 3.3 below.

Theorem 3.3. *With the causal diagram G in Fig. 1, K is not independent with V .*

Therefore, to enable transportable domain adaptation, one needs to train an encoder parameterized by Eqn. 2 while aligning the distributions of v for different domains. Such alignment is done via an adversarial training process, as detailed in Sec. 4 below.

4 METHOD

To learn an ideal encoder $Q(v|x)$ that satisfies the two requirements as defined in Definition 1, we propose to learn an sophisticated encoder $Q(v|x)$ in the form of Eqn. 2 while making sure that the distribution of the causal encodings $v \sim Q(v|x)$ from all domains \mathcal{K} are aligned. Such alignment corresponds to Requirement (2) of Definition 1, i.e., the marginal independence $k \perp\!\!\!\perp v$; it ensures

that all labels can be accurately predicted by the shared predictor $P(y|v)$ using Eqn. 1. We achieve this using an additional discriminator $D(k|v)$, which predicts the domain index k given the causal encoding v .

Once an ideal encoder $Q(v|x)$ is trained, one can then use Eqn. 1 to predict y . Below, we start by introducing our CADA’s causal encoder $Q(v|x)$, predictor $F(y|v)$, and discriminator $D(k|v)$. We can put them together to form a final objective function to perform a minimax optimization.

Causal Encoder $Q(v|x)$. Our causal encoder will take the form of Eqn. 2, which consists of three components, i.e., an intermediate encoder $P(r|x)$, an augmented encoder $P(v|r, x)$, and a data sampler $P(x')$:

- **Intermediate Encoder** $P(r|x)$: The intermediate encoder encodes the input x into the intermediate representation r . To enable sampling of r , this is a *probabilistic* encoder, where sampling $r \sim P(r|x)$ equivalent to

$$r \sim \mathcal{N}(\mu_r(x), \sigma_r^2(x)),$$

where $\mu_r(\cdot)$ and $\sigma_r^2(\cdot)$ denote two neural networks taking x as input and predict the mean and variance of r , respectively. These networks can be trained using the reparameterization trick (Kingma & Welling, 2013).

- **Augmented Encoder** $P(v|r, x')$: The augmented encoder takes as input the intermediate representation r and another input data point $x' \neq x$ as augmented data to predict the preliminary v . Similar to $P(r|x)$, sampling $v \sim P(v|r, x')$ equivalent to

$$v \sim \mathcal{N}(\mu_v(r, x'), \sigma_v^2(r, x')),$$

where $\mu_v(\cdot, \cdot)$ and $\sigma_v^2(\cdot, \cdot)$ denote two neural networks trained using the reparameterization trick (Kingma & Welling, 2013).

- **Data Sampler** $P(x')$: The data sampling uniformly randomly samples data from different domains with different labels. The goal is to include diverse data with different spurious features into the model, such that these spurious features can cancel each other out using the summation $\sum_{x'} P(v|r, x')P(x')$ in Eqn. 2, thereby leading to “more causal” encodings v .

As a result, given the input x , sampling v from our causal encoder is equivalent to first sampling x ’s intermediate representation r from $P(r|x)$, sampling x' from the data sampler $P(x')$, and then sampling v from $P(v|r, x')$. Note that this composed causal encoder $Q(v|x)$ can be trained end-to-end with the reparameterization trick (Kingma & Welling, 2013).

Predictor $F(y|v)$. According to Eqn. 1, our predictor $F(y|v)$ takes as input the causal encoding v from $Q(v|x)$ and predicts the label y . In CADA, $F(y|v)$ is parameterized by a simple multi-layer perceptron (MLP). Note that $F(y|v) = P(y|v)$ in CADA.

Discriminator $D(k|v)$. Our discriminator $D(k|v)$ takes as input the causal encoding v and predicts the domain index k . $D(k|v)$ is crucial in terms of aligning the distributions of causal encodings v from different domains (more details below). Since we focus on DA across continuously indexed domains, $D(k|v)$ will directly *regress* the continuous index k (Wang et al., 2020) rather than performing classification (Ganin et al., 2016).

Final Objective Function. Putting $Q(v|x)$, $F(y|v)$, and $D(k|v)$ together, we can form the following minimax optimization:

$$\min_{Q, F} \max_D V_p(Q, F) - \lambda_d V_d(D, Q), \quad (3)$$

where the instantiations of both terms are **very different** from (Ganin et al., 2016; Wang et al., 2020). Specifically, the **first term**

$$V_p(Q, F) = \frac{1}{N_s} \sum_{(x, y, k) \sim p^s(x, y, k)} \left(-\log \sum_v F(y|v)Q(v|x) \right), \quad (4)$$

measures the *difference* between the *prediction* \hat{y} (computed by Q and F) and the *ground truth* y ; this can be computed as the negative log-likelihood of y , i.e., $-\log \sum_v F(y|v)Q(v|x)$. We compute the average difference over N_s tuples of (x, y, k) sampled from $p^s(x, y, k)$.

Note that to generate the prediction \hat{y} , one has to go through $Q(v|x)$ and $F(y|v)$, with $Q(v|x)$ consisting of three components $P(r|x)$, $P(x')$, and $P(v|r, x')$ in Eqn. 2. Specifically, given an

input-label-index tuple (x, y, k) sampled from the source data distribution, we will first sample r from $P(r|x)$, sample x' from $P(x')$, sample v from $P(v|r, x')$ given the previous sampled r and x' , and then generate prediction \hat{y} from $P(y|v)$ given the sampled v . We then compute the prediction loss for \hat{y} against the label y .

The second term,

$$V_d(D, Q) = \frac{1}{N_{\text{all}}} \sum_{(x, y, k) \sim p(x, y, k)} \left(-\log \sum_v D(k|v)Q(v|x) \right), \quad (5)$$

measures the *difference* between the *predicted* domain index \hat{k} (computed by Q and D) and the *ground-truth* domain index k ; this can be computed as the negative log-likelihood of k , i.e., $-\log \sum_v D(k|v)Q(v|x)$. Similar to Eqn. 4, we compute the average difference over N data points sampled from $p(x, y, k)$. Specifically, given an input-label-index tuple (x, y, k) sampled from the entire data distribution, we first sample v from $Q(v|x)$ by going through $P(r|x)$, $P(x')$, and $P(v|r, x')$; the discriminator $D(k|v)$ then generates the predicted domain index \hat{k} given v .

Two Requirements in Definition 1. The minimax optimization with the objective function Eqn. 3 ensures that two requirements in Definition 1 are satisfied:

- Requirement (1) of Definition 1 is ensured by parameterizing the causal encoder $Q(v|x)$ according to Eqn. 2, which uses two probabilistic neural networks, i.e., the intermediate encoder $P(r|x)$ and the augmented encoder $P(v|r, x')$, and the data sampler $P(x')$.
- Requirement (2) of Definition 1 is encouraged by the adversarial loss, i.e., the minimax optimization; the discriminator $D(k|v)$ will be trained to predict the domain index k , while causal encoder $Q(v|x)$ is trained to fool the discriminator. This adversarial process will try to align the distributions of v across different domains such that $D(k|v)$ cannot accurately predict the domain index k . As shown in (Wang et al., 2020), the solution where $k \perp v$ will be among the equilibria of the minimax optimization in Eqn. 3.

Inference (Prediction). After our CADA is trained using Eqn. 3, one can then make predictions (causal inference) by combining Eqn. 1 and Eqn. 2. Specifically, given the input x , one can predict y using

$$P(y|do(x)) = \sum_v P(y|v) \sum_r P(r|x) \sum_{x'} P(v|r, x')P(x'),$$

where we use Monte Carlo estimation to draw samples from different conditional distributions and aggregate the results to obtain the final prediction (see Alg. 1 in Appendix B for the detailed algorithm).

5 EXPERIMENTS

We evaluated our method, CADA, using a semi-synthetic image dataset, Continuous Colored-MNIST (C2MNIST), along with two real-world medical datasets, Sleep Heart Health Study (SHHS) (Quan et al., 1998) and Multi-Ethnic Study of Atherosclerosis (MESA) (Chen et al., 2014), where continuously shifting spurious features are introduced. These empirical studies corroborate the theoretical discoveries outlined earlier and demonstrate the following:

- Using categorical domain adaptation to align continuously indexed domains with continuously shifting spurious features leads to suboptimal alignment and performance.
- Continuously indexed domain adaptation methods alone tend to align shifting spurious features rather than causal features, and are therefore not effective for domain adaptation with continuously shifting spurious features.
- Causality-based domain adaptation methods alone suffer from covariant shift across domains and are not effective in adaptation across continuously indexed domains.
- Our CADA successfully infer and align causal representations from continuously indexed domains even in the presence of continuously shifting spurious features, thereby significantly improving performance.

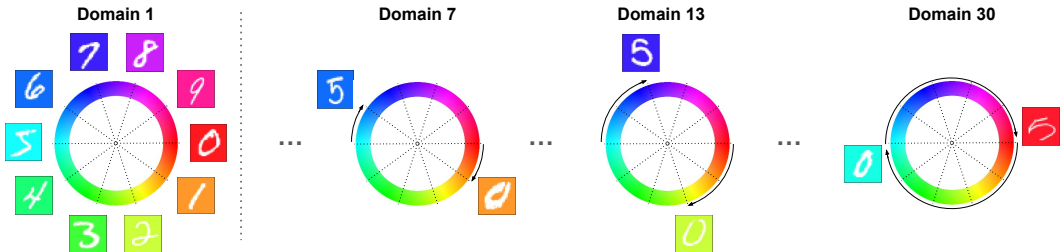


Figure 2: Illustration of the C2MNIST dataset. As shown on the left, the background colors for digit 0 to 9 are evenly separated on the color wheel. As we rotate $6(k - 1)^\circ$ clockwise from the base angles (domain 1), the background colors for domain k shift while still maintaining even separation.

Table 2: **C2MNIST accuracy (%) for CADA and various baselines.** We report the accuracy in the source domains and each target domain range. The intervals in the first row represent the domain range of corresponding domains. The average accuracy across target domains is shown in the last column. We use **bold face** to highlight the best results.

Method	[1, 7) (Source)	[7, 11)	[11, 15)	[15, 19)	[19, 23)	[23, 27)	[27, 31)	Average
Source-Only	100.0	0.1	0.0	0.0	0.0	0.0	0.0	0.0
CUA	97.3	13.25	0.0	0.0	0.0	0.0	0.0	2.2
ADDA	100.0	1.4	0.0	0.0	0.0	0.0	0.0	0.2
DANN	100.0	46.0	5.0	0.0	0.0	0.0	0.0	8.5
CDANN	99.9	76.1	62.0	24.9	9.8	11.5	7.8	32.0
MDD	100.0	66.1	35.5	20.0	9.3	0.5	5.4	22.8
CIDA	100.0	1.8	0.0	0.0	0.0	0.0	0.0	0.3
VOOD	100.0	48.0	9.9	9.9	9.1	9.6	9.4	16.0
CADA (Ours)	100.0	100.0	100.0	100.0	100.0	100.0	82.9	97.1

5.1 BASELINES AND IMPLEMENTATION DETAILS

We compare CADA with state-of-the-art methods in domain adaptation and causal transportation baselines, including Continuous Unsupervised Adaptation (CUA) (Bobu et al., 2018), Adversarial Discriminative Domain Adaptation (ADDA) (Tzeng et al., 2017), Domain Adversarial Neural Network (DANN) (Ganin et al., 2016), Conditional Domain Adversarial Neural Network (CDANN) (Zhao et al., 2017), Margin Disparity Discrepancy (MDD) (Zhang et al., 2019), Continuously Indexed Domain Adaptation (CIDA) (Wang et al., 2020), and Visual Out-of-Distribution Generalization (VOOD) (Mao et al., 2022).

Since the majority of the baselines are not designed for continuously indexed domains, we made slight generalizations to accommodate these baselines. Specifically, for ADDA, MDD and VOOD, data with different domain indices are merged into one source and one target domain; for DANN, CDANN and CUA, the continuous domain spectrum is discretized into multiple disjoint domains, enabling adaptation between multiple source and target domains. In the case of CUA, the model adapts from the source domains to each target domain individually, progressing from the closest target to the farthest one. All methods are implemented in PyTorch (Paszke et al., 2019) with the same neural network architectures and inputs (x and domain index k) for fair comparison.

5.2 CONTINUOUS COLORED-MNIST

Dataset Description. We start from the simple MNIST (LeCun et al., 1998) dataset since the simplicity of the dataset allows us to study the methods in a controlled environment. We adapt the dataset to continuously indexed domain adaptation with shifting spurious features by adding

378
 379
 380
 381
 382
 383
 384
 385
 386
 387
 388
 389
 390
 391
 392
 393
 394
 395
 396
 397
 398
 399
 400
 401
 402
 403
 404
 405
 406
 407
 408
 409
 410
 411
 412
 413
 414
 415
 416
 417
 418
 419
 420
 421
 422
 423
 424
 425
 426
 427
 428
 429
 430
 431

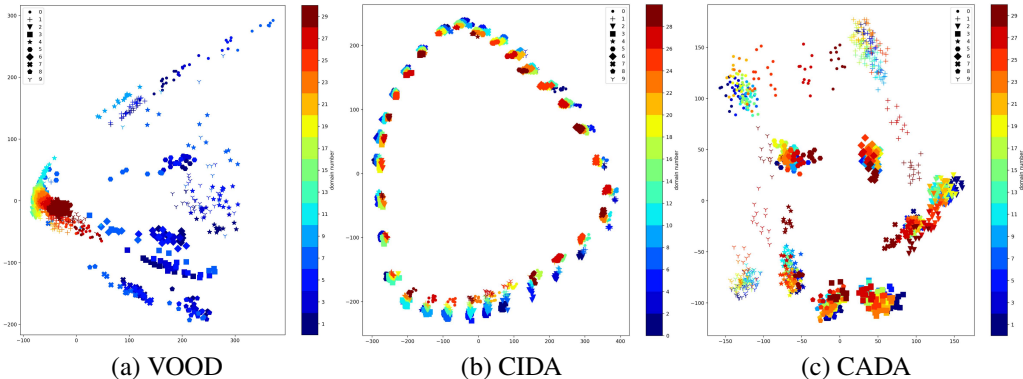


Figure 3: Visualization of learned representations on the C2MNIST dataset, with dimensionality reduction to 2D using principle component analysis (PCA). Domain indices are indicated by color, while data labels are represented by various markers. (a) VOOD’s source- and target-domain embedding distributions are not aligned due to covariate shift, resulting in poor performance in the target domain. (b) CIDA’s source- and target-domain embedding distributions are better aligned compared to VOOD. However, they are not aligned by labels. Specifically, these embeddings form 30 clusters, with each cluster containing embeddings with different labels, resulting in poor classification performance. (c) CADA’s source- and target-domain embedding distributions are aligned by labels. Specifically, these embeddings form 10 clusters, with each cluster containing embeddings with the same label; this makes learning an optimal decision boundary for classification significantly easier, resulting in superior classification performance. See enlarged versions of these figures in Appendix F.

background colors to the digits, where the color depends on both the domain index and the digit, as illustrated in Fig. 2.

We first create a color wheel from the HSV color space as shown in Fig. 2. For $k = 1$, colors are sampled from $0^\circ, 36^\circ, \dots, 324^\circ$ of the color wheel for digit $0, 1, \dots, 9$ respectively. The angles are shown in dotted lines in the figure. For domain $k > 1$, the sampling angles of all the digits are rotated $6(k - 1)^\circ$ clockwise from the base domain $k = 1$. The difference in domain index therefore indicate the distance in the distribution of background colors.

We then treat the domains with $k \leq 6$ as the source domains, and use the remaining ones as the target domains. As a result, for any two distinct digits in the source domains, the ranges their background colors are disjoint, which means that background colors are highly predictive in the source domains. However, these background colors do not generalize to target domains; they are therefore spurious correlations that do not hold across domains. This allows us to verify the empirical performance of different domain adaptation methods.

Accuracy. We further divide the target domains into 6 parts for evaluation based on the distance from the source domains. Table 2 shows the results for different methods. It is evident that in target domains, CUA, ADDA, DANN, and CIDA are completely misled by the continuously shifting spurious features and therefore fail to make predictions in the distant domains. CDANN and MDD, while not entirely wrong in the distant domains, still perform no better than random guessing. While VOOD may theoretically guarantee causal correlation learning, such guarantee break in the presence of covariate shift, which leads to non-positivity in V ’s probability distributions and non-identifiability of the causal interventional distribution $P(V|do(X))$ (Definition 3.2.3 and Definition 3.2.4 of (Pearl et al., 2000)); see Sec. 3.2 for detailed discussion. As a result, VOOD improves upon random guess only in target domains that are the closest to source domains, i.e., domains [7, 11].

Visualization of Latent-Space Representations. To gain more insights on how CADA (1) aligns representation from different domains to remove covariate shift and (2) eliminates continuously shifting spurious features, we visualize the learned representation for two representative baselines: VOOD and CIDA, as well as our model CADA in Fig. 3. The domain indices are indicated by color, while labels are indicated by various markers.

Table 3: **Accuracy (%) for different methods in the SHHS dataset.** The task is to transfer sleep stage prediction models from patients in the age range [44, 53] to [53, 90]. We mark the best result with **bold face** and the second best results with underline.

Method	[44, 53] (Source)	[53, 58]	[58, 63]	[63, 68]	[68, 73]	[73, 78]	[78, 83]	[83, 90]	Average
Source-Only	88.4	62.5	61.8	59.2	59.1	59.7	59.8	59.9	60.2
CUA	85.7	73.6	<u>74.9</u>	<u>73.0</u>	<u>72.7</u>	<u>71.1</u>	<u>67.8</u>	67.2	<u>71.1</u>
ADDA	85.6	<u>73.9</u>	74.1	71.9	71.6	69.9	66.6	65.4	70.1
DANN	87.0	72.4	72.5	69.1	67.5	64.6	60.9	59.9	66.2
CDANN	86.3	72.6	72.8	69.6	68.1	65.5	61.6	60.3	66.7
MDD	91.7	69.8	69.8	70.1	71.2	69.8	67.4	66.6	69.0
CIDA	86.0	<u>72.7</u>	<u>72.4</u>	69.4	69.5	68.6	<u>66.5</u>	65.4	68.9
VOOD	85.5	66.7	66.4	62.5	59.8	56.6	52.9	51.6	58.9
CADA (Ours)	84.3	76.7	77.7	76.1	74.7	72.1	68.9	<u>67.1</u>	72.8

Table 4: **Accuracy (%) for different methods in the MESA dataset.** The task is to transfer sleep stage prediction models from patients in the age range [54, 59] to [89, 92]. We mark the best result with **bold face** and the second best results with underline.

Method	[54, 59] (Source)	[59, 64]	[64, 69]	[69, 74]	[74, 79]	[79, 84]	[84, 89]	[89, 92]	Average
Source-Only	93.3	35.6	35.2	35.3	41.7	55.4	66.6	54.1	46.0
CUA	79.9	75.1	74.1	<u>71.4</u>	70.8	70.1	<u>68.4</u>	65.3	<u>70.9</u>
ADDA	88.7	65.3	70.7	70.7	<u>72.1</u>	<u>72.6</u>	68.3	61.3	68.9
DANN	89.3	59.6	58.6	60.0	63.7	<u>66.8</u>	66.9	66.6	63.1
CDANN	88.5	61.1	60.0	59.4	61.4	64.2	64.6	64.9	62.2
MDD	88.5	60.7	60.2	62.7	67.3	68.5	67.6	<u>67.9</u>	64.9
CIDA	87.8	61.7	60.8	61.2	64.7	66.5	66.0	<u>64.7</u>	63.6
VOOD	95.6	24.3	26.5	34.4	44.7	61.6	56.1	43.0	41.5
CADA (Ours)	80.8	<u>74.3</u>	<u>74.0</u>	72.8	73.2	72.9	72.3	71.1	73.0

- **VOOD: Failing to Remove Covariant Shift.** Fig. 3(a) shows VOOD’s learned representations, which solely focus on causal correlation learning, unable to align source- and target-domain embedding distributions due to covariate shift, resulting in poor performance in the target domain (detailed analysis in Sec. 3.2).
- **CIDA: Failing to Remove Continuously Shifting Spurious Features.** Fig. 3(b) shows the representations from CIDA, a typical continuously indexed domain adaptation method. CIDA aligns source- and target-domain embedding distributions better compared to VOOD. However, they are not aligned by labels. Specifically, these embeddings form 30 clusters, with each cluster containing embeddings with different labels, resulting in poor classification performance.
- **CADA: Successfully Removing Both Covariant Shift and Continuously Shifting Spurious Features.** Fig. 3(c) shows the representations from our CADA. CADA successfully align source- and target-domain embedding distributions by labels. Specifically, these embeddings form 10 clusters, with each cluster containing embeddings with the same label; this makes learning an optimal decision boundary for classification significantly easier, resulting in superior classification performance. For better view, please see the enlarged versions of (a), (b), and (c) in Appendix F.

5.3 HEALTHCARE DATASETS

Dataset Description. We use two medical datasets, SHHS and MESA to evaluate different methods. Both datasets contain records of subjects’ full-night breathing signals and corresponding sleep stage labels for every 30-second segment. Sleep stage labels include “Awake”, “Light Sleep N1”, “Light Sleep N2”, “Deep Sleep”, and “Rapid Eye Movement (REM)”. Given a breathing signal segment x , a common task in sleep studies is to predict the sleep stage label y . While prior studies may consider ‘Light Sleep N1’ and ‘Light Sleep N2’ to be a single stage (Zhao et al., 2017; Wang et al., 2020), we maintain a 5-class classification task in this paper. Among all the subjects’ information, age can serve as a natural domain index. The age range of subjects used is [44, 90] and [54, 92] for SHHS and MESA, respectively. Our SHHS and MESA datasets contain continuously shifting spurious noise to

486 simulate the potential increase in noise due to age-related lower-quality sleeping, breathing disorder
487 (e.g., sleep apnea), etc.

488 **Accuracy.** Table 3 and Table 4 show the accuracy for different methods on SHHS and MESA,
489 respectively. The target domains of both datasets are divided into 7 parts for evaluation based on the
490 distance from the source domains. One observation is that VOOD, as a causal transportation method,
491 shows negative improvement compared to Source-Only (e.g., training the model on source domains
492 and directly use it on target domains without adaptation). While methods that directly use categorical
493 domain adaptation perform poorly in the normal continuously indexed domain adaptation setting,
494 CUA shows better performance than other baselines in our setting. On the other hand, our CADA
495 avoids the influence of continuously shifting spurious correlation, demonstrating stable and good
496 performance in both datasets.

497 6 CONCLUSION

498 In this paper, we identify the problem of continuous spurious shift and propose continuously trans-
499 portable domain adaptation (CADA) as the first general DA method to address this problem. Our
500 theoretical analysis shows that our CADA can better ensure causal transportability across continu-
501 ously indexed domains. Empirical results on both semi-synthetic and real-world medical datasets
502 show that our method outperforms the state-of-the-art DA methods in the face of continuous spurious
503 shift. Interesting future work includes extending the proposed method to multi-dimensional domain
504 indices, more complex shifting spurious features, and other applications beyond healthcare.

505 REFERENCES

- 506 Martin Arjovsky, Léon Bottou, Ishaan Gulrajani, and David Lopez-Paz. Invariant risk minimization.
507 *arXiv preprint arXiv:1907.02893*, 2019.
- 508 Elias Bareinboim and Judea Pearl. A general algorithm for deciding transportability of experimental
509 results. *Journal of causal Inference*, 1:107–134, 2013.
- 510 Elias Bareinboim and Judea Pearl. Transportability from multiple environments with limited experi-
511 ments: Completeness results. *Advances in neural information processing systems*, 27, 2014.
- 512 Elias Bareinboim and Judea Pearl. Causal inference and the data-fusion problem. *Proceedings of the*
513 *National Academy of Sciences*, 113:7345–7352, 2016.
- 514 Shai Ben-David, John Blitzer, Koby Crammer, Alex Kulesza, Fernando Pereira, and Jennifer Wortman
515 Vaughan. A theory of learning from different domains. *Machine learning*, 79:151–175, 2010.
- 516 Andreea Bobu, Eric Tzeng, Judy Hoffman, and Trevor Darrell. Adapting to continuously shifting
517 domains. 2018.
- 518 Peter Bühlmann. Invariance, causality and robustness. 2020.
- 519 Xiaoli Chen, Rui Wang, Phyllis Zee, Pamela Lutsey, Sogol Javaheri, Carmela Alcántara, Chandra
520 Jackson, Michelle Williams, and Susan Redline. Racial/ethnic differences in sleep disturbances:
521 The multi-ethnic study of atherosclerosis (mesa). *Sleep*, 38, 11 2014. doi: 10.5665/sleep.4732.
- 522 Juan Correa and Elias Bareinboim. General transportability of soft interventions: Completeness
523 results. *Advances in Neural Information Processing Systems*, 33:10902–10912, 2020.
- 524 Juan D Correa and Elias Bareinboim. From statistical transportability to estimating the effect of
525 stochastic interventions. In *IJCAI*, pp. 1661–1667, 2019.
- 526 Gabriela Csurka. Domain adaptation for visual applications: A comprehensive survey. *arXiv preprint*
527 *arXiv:1702.05374*, 2017.
- 528 Abolfazl Farahani, Sahar Voghoei, Khaled Rasheed, and Hamid R Arabnia. A brief review of domain
529 adaptation. *Advances in data science and information engineering: proceedings from ICDATA*
530 *2020 and IKE 2020*, pp. 877–894, 2021.

- 540 Yaroslav Ganin, Evgeniya Ustinova, Hana Ajakan, Pascal Germain, Hugo Larochelle, Franccois
541 Laviolette, Mario Marchand, and Victor Lempitsky. Domain-adversarial training of neural networks.
542 *JMLR*, 17(1):2096–2030, 2016.
- 543
- 544 Arthur Gretton, Alex Smola, Jiayuan Huang, Marcel Schmittfull, Karsten Borgwardt, Bernhard
545 Schölkopf, et al. Covariate shift by kernel mean matching. *Dataset shift in machine learning*, 3(4):
546 5, 2009.
- 547 Diederik P Kingma and Max Welling. Auto-encoding variational bayes. *arXiv preprint*
548 *arXiv:1312.6114*, 2013.
- 549
- 550 Ananya Kumar, Tengyu Ma, and Percy Liang. Understanding self-training for gradual domain
551 adaptation. In *International Conference on Machine Learning*, pp. 5468–5479. PMLR, 2020.
- 552 Yann LeCun, Léon Bottou, Yoshua Bengio, and Patrick Haffner. Gradient-based learning applied to
553 document recognition. *Proceedings of the IEEE*, 86(11):2278–2324, 1998.
- 554
- 555 Zachary Lipton, Yu-Xiang Wang, and Alexander Smola. Detecting and correcting for label shift with
556 black box predictors. In *International conference on machine learning*, pp. 3122–3130. PMLR,
557 2018.
- 558 Tianyi Liu, Zihao Xu, Hao He, Guang-Yuan Hao, Guang-He Lee, and Hao Wang. Taxonomy-
559 structured domain adaptation. In *International Conference on on Machine Learning*, 2023.
- 560
- 561 Sara Magliacane, Thijs Van Ommen, Tom Claassen, Stephan Bongers, Philip Versteeg, and Joris M
562 Mooij. Domain adaptation by using causal inference to predict invariant conditional distributions.
563 *Advances in neural information processing systems*, 31, 2018.
- 564 Divyat Mahajan, Shruti Tople, and Amit Sharma. Domain generalization using causal matching. In
565 *International Conference on Machine Learning*, pp. 7313–7324. PMLR, 2021.
- 566
- 567 Chengzhi Mao, Augustine Cha, Amogh Gupta, Hao Wang, Junfeng Yang, and Carl Vondrick.
568 Generative interventions for causal learning. In *Proceedings of the IEEE/CVF Conference on*
569 *Computer Vision and Pattern Recognition*, pp. 3947–3956, 2021.
- 570 Chengzhi Mao, Kevin Xia, James Wang, Hao Wang, Junfeng Yang, Elias Bareinboim, and Carl
571 Vondrick. Causal transportability for visual recognition. In *CVPR*, 2022.
- 572
- 573 Le Thanh Nguyen-Meidine, Atif Belal, Madhu Kiran, Jose Dolz, Louis-Antoine Blais-Morin, and
574 Eric Granger. Unsupervised multi-target domain adaptation through knowledge distillation. In
575 *Proceedings of the IEEE/CVF Winter Conference on Applications of Computer Vision*, pp. 1339–
576 1347, 2021.
- 577 Sinno Jialin Pan, Ivor W Tsang, James T Kwok, and Qiang Yang. Domain adaptation via transfer
578 component analysis. *TNN*, 22(2):199–210, 2010.
- 579
- 580 Adam Paszke, Sam Gross, Francisco Massa, Adam Lerer, James Bradbury, Gregory Chanan, Trevor
581 Killeen, Zeming Lin, Natalia Gimelshein, Luca Antiga, Alban Desmaison, Andreas Kopf, Edward
582 Yang, Zachary DeVito, Martin Raison, Alykhan Tejani, Sasank Chilamkurthy, Benoit Steiner,
583 Lu Fang, Junjie Bai, and Soumith Chintala. Pytorch: An imperative style, high-performance
584 deep learning library. In H. Wallach, H. Larochelle, A. Beygelzimer, F. d'Alché-Buc, E. Fox, and
585 R. Garnett (eds.), *Advances in Neural Information Processing Systems*, volume 32. Curran Asso-
586 ciates, Inc., 2019. URL [https://proceedings.neurips.cc/paper_files/paper/
2019/file/bdbca288fee7f92f2bfa9f7012727740-Paper.pdf](https://proceedings.neurips.cc/paper_files/paper/2019/file/bdbca288fee7f92f2bfa9f7012727740-Paper.pdf).
- 587
- 588 Judea Pearl. *Causality*. Cambridge University Press, 2 edition, 2009.
- 589
- 590 Judea Pearl and Elias Bareinboim. Transportability of causal and statistical relations: A formal
591 approach. In *Proceedings of the AAAI Conference on Artificial Intelligence*, volume 25, pp.
592 247–254, 2011.
- 593
- Judea Pearl et al. Models, reasoning and inference. *Cambridge, UK: CambridgeUniversityPress*, 19
(2):3, 2000.

- 594 Xingchao Peng, Qinxun Bai, Xide Xia, Zijun Huang, Kate Saenko, and Bo Wang. Moment matching
595 for multi-source domain adaptation. In *Proceedings of the IEEE/CVF International Conference on*
596 *Computer Vision*, pp. 1406–1415, 2019.
- 597
598 Viraj Prabhu, Shivam Khare, Deeksha Kartik, and Judy Hoffman. Sentry: Selective entropy opti-
599 mization via committee consistency for unsupervised domain adaptation. In *Proceedings of the*
600 *IEEE/CVF International Conference on Computer Vision*, pp. 8558–8567, 2021.
- 601
602 Stuart Quan, Barbara Howard, Conrad Iber, James Kiley, F. Nieto, George O’Connor, David Rapoport,
603 Susan Redline, John Robbins, Jonathan Samet, and ‡Patricia Wahl. The sleep heart health study:
604 Design, rationale, and methods. *Sleep*, 20:1077–85, 01 1998. doi: 10.1093/sleep/20.12.1077.
- 605
606 Mateo Rojas-Carulla, Bernhard Schölkopf, Richard Turner, and Jonas Peters. Invariant models for
causal transfer learning. *The Journal of Machine Learning Research*, 19(1):1309–1342, 2018.
- 607
608 Hidetoshi Shimodaira. Improving predictive inference under covariate shift by weighting the log-
likelihood function. *Journal of statistical planning and inference*, 90(2):227–244, 2000.
- 609
610 Baochen Sun and Kate Saenko. Deep CORAL: correlation alignment for deep domain adaptation. In
611 *ICCV workshop on Transferring and Adapting Source Knowledge in Computer Vision (TASK-CV)*,
612 pp. 443–450, 2016.
- 613
614 Eric Tzeng, Judy Hoffman, Ning Zhang, Kate Saenko, and Trevor Darrell. Deep domain confusion:
Maximizing for domain invariance. *arXiv preprint arXiv:1412.3474*, 2014.
- 615
616 Eric Tzeng, Judy Hoffman, Kate Saenko, and Trevor Darrell. Adversarial discriminative domain
617 adaptation. In *CVPR*, pp. 7167–7176, 2017.
- 618
619 Hao Wang, Hao He, and Dina Katabi. Continuously indexed domain adaptation. In *ICML*, 2020.
- 620
621 Zihao Xu, Hao He, Guang-He Lee, Yuyang Wang, and Hao Wang. Graph-relational domain adaptation.
In *ICLR*, 2022.
- 622
623 Zihao Xu, Guang-Yuan Hao, Hao He, and Hao Wang. Domain-indexing variational bayes: Inter-
624 pretable domain index for domain adaptation. In *International Conference on Learning Representations*, 2023.
- 625
626 Zhongqi Yue, Qianru Sun, Xian-Sheng Hua, and Hanwang Zhang. Transporting causal mechanisms
627 for unsupervised domain adaptation. In *Proceedings of the IEEE/CVF International Conference*
628 *on Computer Vision*, pp. 8599–8608, 2021.
- 629
630 Yuchen Zhang, Tianle Liu, Mingsheng Long, and Michael I Jordan. Bridging theory and algorithm
for domain adaptation. *arXiv preprint arXiv:1904.05801*, 2019.
- 631
632 Mingmin Zhao, Shichao Yue, Dina Katabi, Tommi S. Jaakkola, and Matt T. Bianchi. Learning sleep
633 stages from radio signals: A conditional adversarial architecture. In *ICML*, pp. 4100–4109, 2017.
- 634
635 Yang Zou, Zhiding Yu, B.V.K. Vijaya Kumar, and Jinsong Wang. Unsupervised domain adaptation for
636 semantic segmentation via class-balanced self-training. In *Proceedings of the European Conference*
637 *on Computer Vision (ECCV)*, September 2018.
- 638
639
640
641
642
643
644
645
646
647

A PROOFS

Theorem A.1 (Transportability of $P(v|do(x))$). *With the causal diagram in Fig. 1, the causal relation $P(v|do(x))$ is transportable from domain k_1 to k_2 for any $k_1 \neq k_2$.*

Proof. Given that R satisfies the front-door criterion (Pearl, 2009), we can then use the front-door adjustment formula to obtain:

$$P(v|do(x)) = \sum_r P(r|x) \sum_{x'} P(v|r, x')P(x').$$

By the definition of trivial transportability (Pearl & Bareinboim, 2011), since $P(v|do(x))$ is identifiable, we have that $P(v|do(x))$ is transportable. \square

Theorem A.2 (Transportability of $P(y|do(X))$). *With the causal diagram in Fig. 1, the causal relation $P(y|do(x))$ is trivially transportable from domain k_1 to k_2 for any $k_1 \neq k_2$ using:*

$$P(y|do(x)) = \sum_v P(y|v)Q(v|x), \quad (6)$$

where $Q(v|x)$ is an probabilistic encoder generating encoding v given the input x . It is constructed as

$$Q(v|x) = \sum_r P(r|x) \sum_{x'} P(v|r, x')P(x'). \quad (7)$$

Proof. Using the chain rule we have that $P(y|do(x)) = \sum_v P(y|v)P(v|do(x))$, where $P(v|do(x))$ is given by Theorem A.1. Denoting $P(v|do(x))$ as $Q(v|x)$ concludes the proof. \square

Theorem A.3. *With the causal diagram G in Fig. 1, K is not independent with V .*

Proof. This is straightforward given that $K \not\perp\!\!\!\perp V$ in $G_{\overline{X}}$. \square

B INFERENCE ALGORITHM OF CADA

Alg. 1 shows details for CADA’s inference (prediction) process.

Algorithm 1 Inference (Prediction) Using CADA

```

1: Input: Query  $x$ , data distribution  $\mathcal{D}$  over  $\{(x, y, k)\}$ , causal encoder  $Q(v|x)$  consisting of the
   intermediate encoder  $P(r|x)$  and the augmented encoder  $P(v|r, x')$ . Numbers of samples for  $r$ ,
    $x'$ , and  $v$ , i.e.,  $N_r$ ,  $N_x$ , and  $N_v$ .
2: for  $i = 1, \dots, N_r$  do
3:   Sample  $r^{(i)} \sim P(r|x)$ .
4:   for  $j = 1, \dots, N_x$  do
5:     Sample from the data distribution:  $\mathbf{x}'^{(ij)} \sim P(x')$ .
6:     for  $m = 1, \dots, N_v$  do
7:       Sample  $v^{(ijm)} \sim P(v|r^{(i)}, \mathbf{x}'^{(ij)})$ .
8:     end for
9:   end for
10: end for
11: Compute the causal effect for each class:  $P(y|do(x)) =$ 
     $\frac{1}{N_r N_x N_v} \sum_{i=1}^{N_r} \sum_{j=1}^{N_x} \sum_{m=1}^{N_v} P(y|v^{(ijm)})$ .
12: Output: Class prediction  $\hat{y} = \operatorname{argmax}_y P(y|do(x))$ .

```

C MORE IMPLEMENTATION DETAILS

Compute Resources. All methods are implemented with PyTorch (Paszke et al., 2019), and run on a single NVIDIA RTX A5000 GPU.

Training Process. For the C2MNIST dataset, all models are trained for 1600 epochs. Our CADA framework’s training process is divided into four stages of 400 epochs each, transferring progressively from the previously learned domain to the next: [7, 13), [13, 19), [19, 25) and [25, 31). For healthcare datasets, all models are trained for 50 epochs. Our CADA framework’s training process occurs in a single stage, transferring from the source domains to all target domains. We applied a simple grid search to determine the optimal configuration, which is fixed across methods for fair comparison.

Model Architectures. For fair comparison, we adopt the same backbone neural network architectures for baseline methods and CADA within the same dataset. In C2MNIST, we use the same multi-layer perceptron as in CIDA (Wang et al., 2020), with the hidden dimension set to 800. For healthcare datasets, we adopt the same setting as in CIDA for sleep learning, with the hidden dimension set to 384.

D LIMITATION

Our method currently only works with image and time series data. Additional work is needed to extend it to other modalities, such as text, videos, and audio.

E BROADER IMPACT

While our method for domain adaptation shows promise in transferring knowledge across continuously indexed domains and enhancing performance in medical datasets, it is important to consider its broader societal impacts.

A possible negative societal impact is that our method requires access to detailed domain-specific data, which might include sensitive personal information such as patient ages and medical histories. Misuse or data breaches could lead to significant privacy violations. To address this, we propose incorporating privacy-preserving techniques such as differential privacy or federated learning to ensure that sensitive data is protected and not directly exposed during the training and adaptation processes.

F ENLARGED FIGURES FOR REPRESENTATION VISUALIZATION

Fig. 4, Fig. 5, and Fig. 6 are the enlarged versions of Fig. 3(a), Fig. 3(b), and Fig. 3(c) in the main paper.

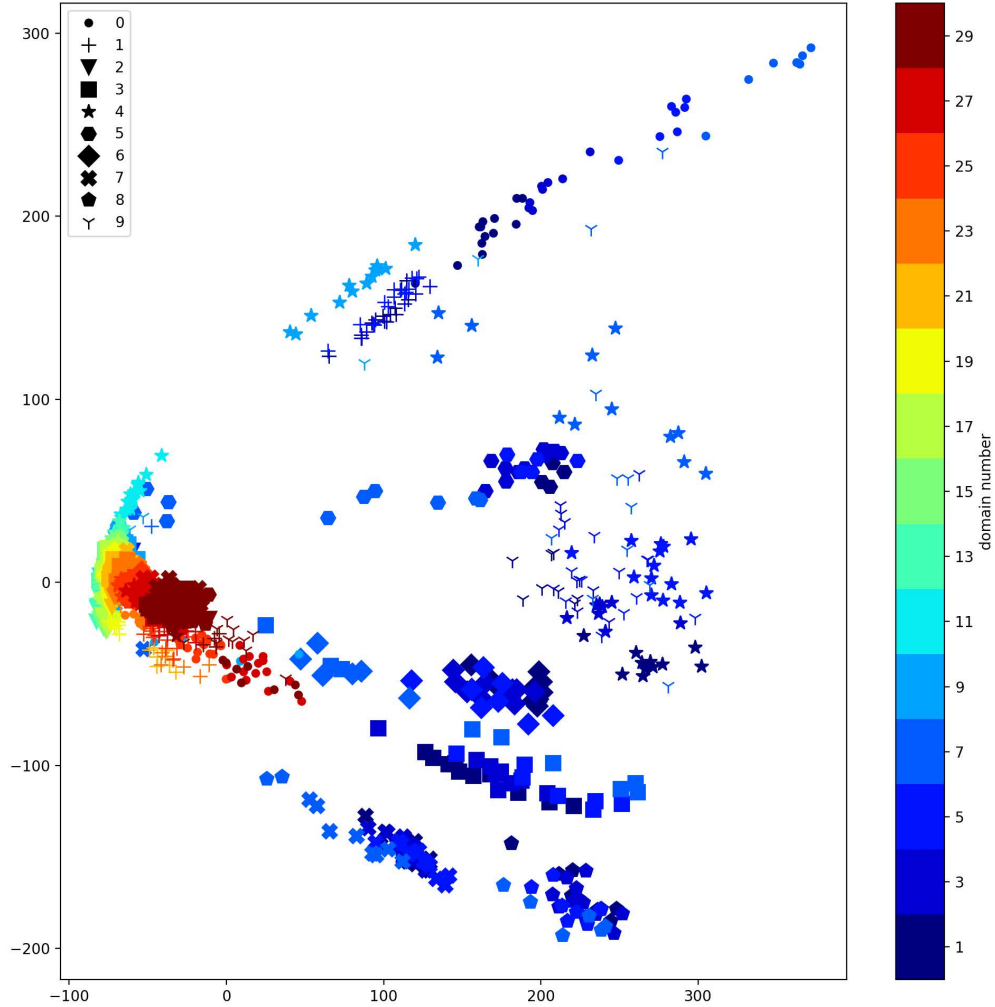


Figure 4: Enlarged version of Fig. 3(a): Visualization of VOOD's representations.

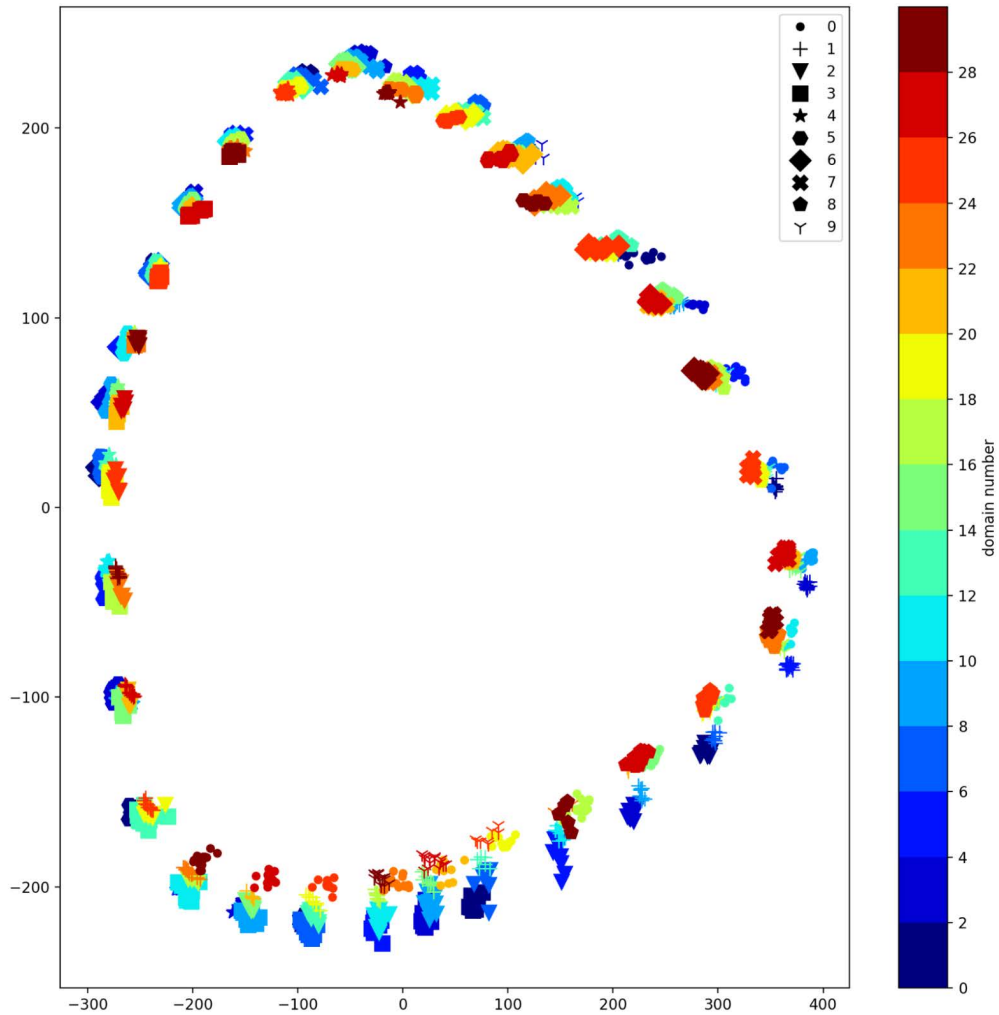


Figure 5: Enlarged version of Fig. 3(b): Visualization of CIDA's representations.

864
865
866
867
868
869
870
871
872
873
874
875
876
877
878
879
880
881
882
883
884
885
886
887
888
889
890
891
892
893
894
895
896
897
898
899
900
901
902
903
904
905
906
907
908
909
910
911
912
913
914
915
916
917

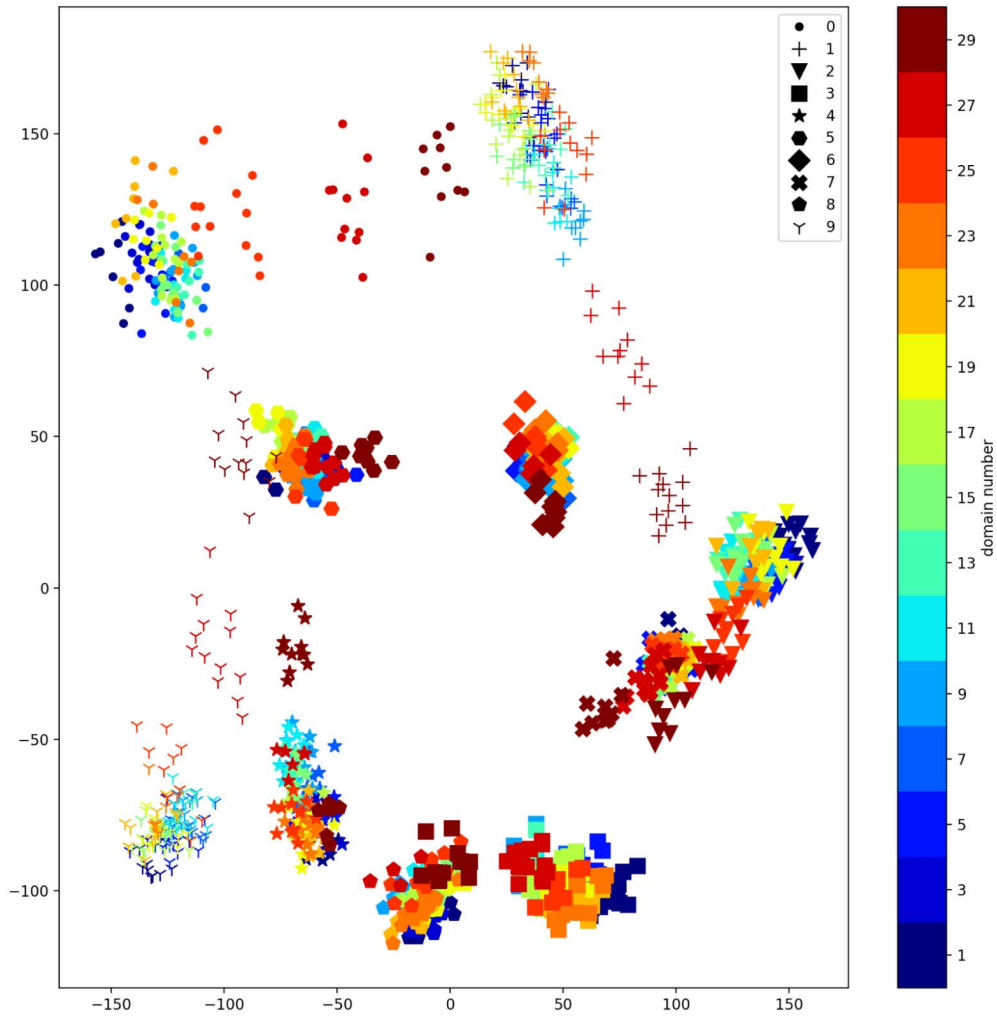


Figure 6: Enlarged version of Fig. 3(c): Visualization of CADA’s representations.